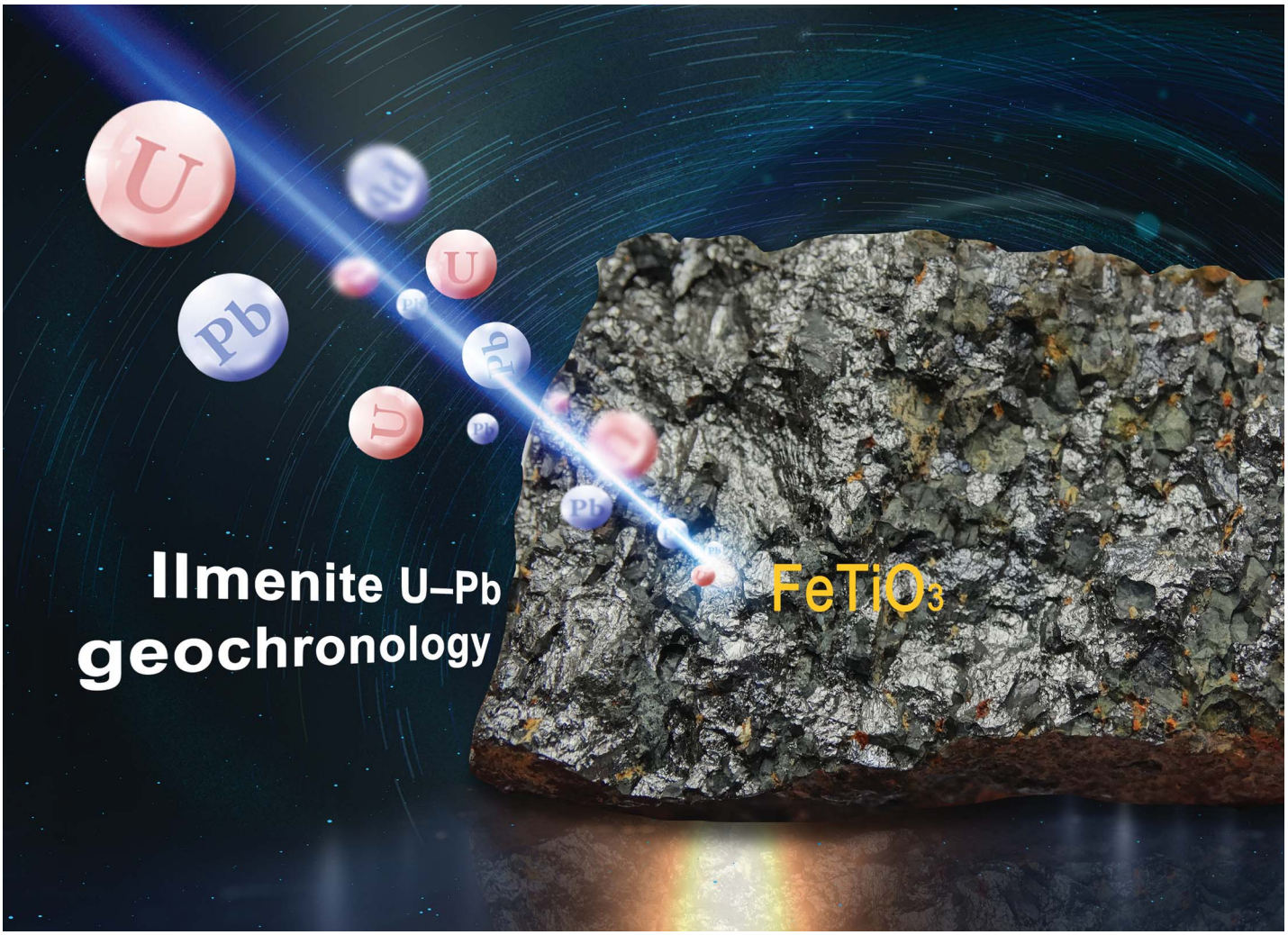

Showcasing research from Dr. Yanwen Tang's laboratory, State Key Laboratory of Ore Deposit Geochemistry, Institute of Geochemistry, Chinese Academy of Sciences, Guiyang, China.

A new appraisal of ilmenite U–Pb dating method by LA-SF-ICP-MS

Besides being a major source of titanium metal, ilmenite is an important geochronometer in various rocks and deposits. The use of LA-SF-ICP-MS for ilmenite dating is an impressive technological approach, which allows rapid dating with spot sizes of ~60 μm and low U and Pb contents in the tens to hundreds of ppb range. The calibration of U-Pb isotopes using zircon 91500 to achieve accurate ages with minimal age offsets for ilmenite samples is a crucial aspect of this methodology. Three ilmenites are proposed as reference materials in the future.

As featured in:

See Yanwen Tang, Tingguang Lan *et al.*, *J. Anal. At. Spectrom.*, 2024, **39**, 109.

ROYAL SOCIETY OF CHEMISTRY

rsc.li/jaas

Registered charity number: 207890

JAAS

ROYAL SOCIETY OF CHEMISTRY

PAPER

View Article Online
View Journal | View Issue

Cite this: *J. Anal. At. Spectrom.*, 2024, **39**, 109

A new appraisal of ilmenite U–Pb dating method by LA-SF-ICP-MS†

Yanwen Tang, [a] Tingguang Lan,[a] Jianfeng Gao,[a] Zhongjie Bai,*[a] Xiaowen Huang,*[a] Junjie Han[a] and Na Liu[ab]

Titanium (Ti) is a crucial metal with wide-ranging applications in various industries. Ilmenite minerals are the main source of Ti metal. As a valuable petrogenetic indicator and geochronometer, ilmenite mineral occurs commonly in igneous and metamorphic rocks and different types of deposits (*e.g.*, Fe–Ti oxide, diamonds, and placer deposits). Ilmenite U–Pb geochronology started by isotope dilution-thermal ionization mass spectrometry thirty years ago and by *in situ* methods recently due to low U and Pb concentrations. A constrained calibration method has been established using rutile TB-1 due to the lack of reference material (RM). However, rutile (*e.g.*, RMJG) cannot be a primary standard in all our analyses. Thus, a new primary standard and accurate calibration method for further applications is urgently needed. By laser ablation sector field inductively coupled plasma mass spectrometry (LA-SF-ICP-MS), optimizing ablation settings and adding N_2 (~3.0 mL min^{-1}) have been employed to minimize the matrix effects between zircon 91500 and ilmenite. Thus, zircon 91500 can be utilized as a RM to measure the Pb/U ratio in ilmenite. Zircon 91500 has a similar U–Pb fractionation and average normalized Pb/U ratio with ilmenite BC269, instead of rutile RMJG, probably owing to the different ablation settings used by us compared to the two previous studies. More accurate ages with much smaller age offsets of ≤1.6% were obtained for the five ilmenite samples calibrated by zircon 91500 compared to those calibrated by Ti- and Fe-bearing minerals, including rutile RMJG, garnet PL-57, and wolframite YGX. These results demonstrate that the direct calibration method used here with 91500 as an external standard is effective for *in situ* U–Pb dating of ilmenite samples under a wide range of ablation settings, *i.e.*, spot sizes varying from 44 to 120 μm, repetition rate from 5 to 10 Hz, and laser fluences from 3 to 4 J cm^{-2}. HG79, XL32333, and BC269 have high U and Pb contents and can be utilized as potential RMs for ilmenite minerals. This approach offers new insights into understanding the diagenetic and ore-forming processes related to ilmenite minerals.

Received 27th June 2023
Accepted 6th October 2023

DOI: 10.1039/d3ja00209h

rsc.li/jaas

1. Introduction

Titanium (Ti) metal has unique properties, such as low density, high strength, and high resistance to heat and corrosion, and thus, has become a crucial feedstock for a wide variety of industrial uses, *e.g.*, aerospace, armor, medicine, marine hardware, national defense, metallurgy, and functional materials.[1,2] As two important Ti-bearing minerals, rutile and ilmenite have a TiO_2 content of up to 100% and 52.7%, respectively. However, ilmenite deposits are more common than rutile in nature and account for about 90% of the world's consumption of titanium minerals.[2] Thus, ilmenite mineral plays a more important role than rutile as a source of Ti metal.

Ilmenite is a common accessory phase in a variety of igneous and metamorphic rocks, as well as magmatic and hydrothermal Fe and Fe–Ti oxide, diamonds, placer, and skarn deposits.[1,3–5] Ilmenite is a valuable petrogenetic indicator to constrain oxygen fugacity, magnetic properties, pressure, and temperature, or to trace its sources.[4,6–8] It occurs as inclusions or as a product of the decomposition or oxidation-exsolution of the different Fe–Ti oxide pairs in solid solutions, which can reflect their cooling histories and play an important role in understanding the evolution and formation process of provenance rocks or deposits.[9,10] Accordingly, the study of the composition of ilmenite, *e.g.*, major and trace elements, by EMPA and LA-ICPMS has been the subject of many studies.[10–13]

Ilmenite is a stable mineral phase and can be preserved well in the natural environment,[5,10,13] unless it suffers high-grade metamorphic–hydrothermal processes.[14] Ilmenite mineral is also a reliable geochronometer, which can be utilized to constrain the formation age of provenance rocks (*e.g.*, metamorphic rock and kimberlites),[14,15] or as the main ore mineral to

[a]*State Key Laboratory of Ore Deposit Geochemistry, Institute of Geochemistry, Chinese Academy of Sciences, Guiyang, 550081, China. E-mail: baizhongjie@vip.gyig.ac.cn; huangxiaowen@mail.gyig.ac.cn*

[b]*University of Chinese Academy of Sciences, Beijing 100049, China*

† Electronic supplementary information (ESI) available. See DOI: https://doi.org/10.1039/d3ja00209h

directly date the timing of mineralization or fluid-related processes,[16] or to resolve the debate that ilmenite is a phenocryst or xenocryst phase in kimberlites.[15] However, the closure temperature to Pb diffusion in ilmenite is unknown so it is difficult to assess the effects of such conditions in detail.[15]

U–Pb ilmenite geochronology has been published in only a few reports because uranium and lead concentrations in ilmenite are both in the range of tens to hundreds of ppb, and the results can be seriously affected by Pb blanks.[14,15,17] Isotope dilution-thermal ionization mass spectrometry (ID-TIMS) for the U–Pb dating of ilmenite has been reported and verified since Burton and O'Nions (1990) and Noyes *et al.* (2011).[14,15] Although the advantage of using a dating method that employs bulk samples is low detection limits and higher precision, it requires more time and sample consumption, higher costs, and is easily affected by the presence of U- and Pb-rich micro-inclusions or alteration phases in which U–Pb isotope systems could be reset.[14,16] LA-ICP-MS was introduced for direct U–Pb dating of U-rich minerals (*e.g.*, zircon) in 1993,[18] and has become popular due to high efficiency, high spatial resolution, and low capital costs. Particularly, some special settings applied in this method can obtain a higher sensitivity/background ratio, including adding N_2, H_2, and water vapor to improve the sensitivity,[19–21] and/or by using a large spot size to enhance signal intensity.[17] Thus, laser ablation (quadrupole/sector field/multi-collector) inductively coupled plasma mass spectrometry (LA-Q/SF/MC-ICP-MS) can analyze ilmenite minerals with low U and Pb concentrations.[17] Previous studies have confirmed that ilmenite is amenable to U–Pb geochronology and offers new insight into understanding diagenetic and ore-forming processes.[14,15,17]

Non-matrix matched calibrations have increasingly been used in LA-ICP-MS U–Pb analysis owing to a lack of matrix-matched reference materials (RMs), *e.g.*, NIST 610 for zircon, monazite, and xenotime;[22] NIST 612 for cassiterite;[23] Plesovice zircon for allanite;[24] zircon 91500 for rutile and garnet;[25–27] zircon 91500 and schorlomite for vesuvianite;[28,29] wolframite YGX for ferberite, hübnerite, and scheelite;[30,31] and xenotime XN01 for bastnaesite.[32] However, matrix effects exist for most of the above minerals due to different ablation behaviors, and thus, special conditions have been employed to reduce matrix effects, including adding water vapor and N_2,[21,22,32] using a large spot size of ≥44 μm,[25] as well as using a low laser sampling rate, a low energy density, short ablation times (~30 s),[23,33] and shorter wavelength of ablation laser.[34]

Rutile TB-1 has been used as a non-matrix-matched primary standard instead of Mud Tank zircon and BCR-2g to calibrate U/Pb ratios and obtain the most accurate U–Pb ages within analytical uncertainties for ilmenite samples by LA-ICP-MS due to the lack of matrix-matched RMs.[17] Generally, RMs that are valid in all or most ablation settings would be preferred. However, such materials are difficult to find due to matrix effects (*e.g.*, variable ablation rates) even among the zircon samples and matrix-matched RMs.[35,36] The in-house rutile TB-1 has a similar normalized $^{206}Pb/^{238}U$ ratio with ilmenite in an optimized ablation setting, but it has not been widely distributed as a potential RM. Moreover, another RM rutile RMJG (1750.1 ± 4.7 Ma)[37] is not suitable for ilmenite samples as shown by our analysis below. Therefore, ilmenite U–Pb dating needs a new calibration method for wide-ranging applications.

In this study, several ilmenite samples with relatively high U and Pb contents and a wide range of formation ages from 2054 to 196 Ma were selected for methodological analysis to (1) find a suitable RM for *in situ* U–Pb dating of ilmenite; (2) evaluate this RM in most possible ablation settings; and (3) establish an accurate calibration method.

2. Experimental

2.1 LA-SF-ICP-MS

Reflected light observations were performed to identify the ilmenite samples. Backscattered electron (BSE) images were collected to identify the internal textures of the ilmenite sample XKS and to help interpret ages. A JSM-7800F field emission scanning electron microscope was used at the State Key Laboratory of Ore Deposit Geochemistry (SKLODG), Institute of Geochemistry, Chinese Academy of Sciences (IGCAS), Guiyang, China. The analytical conditions are listed in the BSE images.

All ilmenite analyses were performed on a GeoLasPro 193 nm ArF excimer laser (CompexPro 102F, Coherent), coupled to an Element XR sector field ICP-MS (Thermo Fisher Scientific, USA) for U–Pb dating at the SKLODG, IGCAS, Guiyang, China. The standard cylinder ablation cell was optimized with a resin mold to get a smaller volume and offer a fast washout of the aerosol. The analyses were performed on spot ablation diameters of 32, 44, 60, 90, and 120 μm; repetition rates of 5, 6, or 10 Hz; and laser fluences of 3 and 4 J cm^{-2}. Systematic screening with spot analyses was also performed on these samples to aim for some high U and low Pb areas before detailed analyses. Helium was used as the carrier gas. Small amounts of nitrogen (~3 mL min^{-1}) were added to the helium gas to increase the sensitivity *via* a simple Y junction downstream of the sample cell and then mixed with argon *via* a T-connector before going into the ICP-MS. NIST SRM 612 glass was used for tuning where the U/Th ratios were kept at ~1.0. Samples and standards in small epoxy mounts (~1 cm) were placed together in the center to minimize the position effect. Each spot analysis includes an approximate 20 s background and 30 s sample data acquisition. A pre-ablation of ~8 pulses was performed to remove Pb contamination from the sample surface. In addition, line scanning mode was also performed in the verification experiment, *i.e.*, using the same laser fluence as with spot analysis, scanning speed of 1 μm s^{-1}, and repetition rate of 5, 6, and 10 Hz. Only smooth signals were saved to preclude high amounts of common lead from fluid inclusion or micro-minerals (*e.g.*, sulfide). The dwell times for each mass scan were 3 ms for ^{202}Hg, ^{204}Pb, ^{208}Pb, ^{232}Th, 15 ms for ^{206}Pb, ^{238}U, and 25 ms for ^{207}Pb, respectively.

Three experiments were arranged as:

(1) By finding a suitable primary standard for accurate U–Pb dating of three ilmenite samples from several known RMs. A normal ablation setting was used, *i.e.*, a laser spot size of 60 μm, repetition rates of 6 or 10 Hz, and energy densities of 4 J cm^{-2}. The high repetition rate of 10 Hz was only to fit the samples with low U and Pb contents.

Table 1 Analytical conditions and several primary standards used in the three experiments[a]

Geolas Pro 193 nm laser ablation system	
Energy density	3, 4 J cm^{-2}
Spot size	32, 44, 60, 90 and 120 μm
Laser frequency	5, 6, 10 Hz
Ablation cell gas	Helium (0.45 L min^{-1})
Thermo Fisher Scientific Finnigan element XR ICP-MS	
Power	1230 W
Plasma gas flow rate	16.0 L min^{-1}
Auxiliary gas flow rate	0.85–0.95 L min^{-1}
Scan type	EScan
Detector mode	Dual
Dwell times (ms)	3 ms for ^{202}Hg, ^{204}Pb, ^{208}Pb, ^{232}Th; 15 ms for ^{206}Pb, ^{238}U; 25 ms for ^{207}Pb
Addition nitrogen to increase the sensitivity	3 mL min^{-1}

Experiment	Analytical conditions	Primary standards	Ilmenite sample
1	60μm4J6, 10Hz450He3N_2	Rutile RMJG, zircon 91500, wolframite YGX, and garnet PL57	HG79, XL32333, BC269
2	44, 60, 90, 120 μm3, 4J5, 6, 10Hz450He3N_2	Rutile RMJG, zircon 91500	HG79
3	32, 44, 60μm4J6Hz450He3N_2	Rutile RMJG, zircon 91500	XL32333, BC28, BC269, XKS

[a] Note: J cm^{-2}, 0.45 L min^{-1} of helium, and 3 mL min^{-1} of N_2 are abbreviated as J, 450He, and 3N_2 in tables and figures. Primary standards were used to calibrate Pb/Pb and Pb/U ratios for ilmenite samples.

(2) Using a well-characterized ilmenite sample HG79, which has relatively high U and Pb contents, to verify this "suitable" primary standard and establish an accurate U–Pb dating method in different analysis settings. A wide range of ablation settings, *i.e.*, laser spot sizes varying from 44 to 120 μm; repetition rates of 5, 6, and 10 Hz; and energy densities of 3 and 4 J cm^{-2}, were mainly used to satisfy the signal for ^{206}Pb, ^{207}Pb, and ^{238}U and fit the potential ilmenite samples in future analyses.

(3) By applying this primary standard and calibration method to several ilmenite samples, especially an unknown ilmenite sample, XKS. The ablation settings of 44 and 60 μm; 4 J cm^{-2}; and 6 Hz were employed to fit ilmenite samples for application.

The analytical conditions are summarized in Table 1.

2.2 Calibration strategy and data reduction

The time-dependent drifts of U–Pb isotopic ratios were corrected with a standard-sample bracketing procedure, *i.e.*, NIST612/NIST614 + 291 500 + 2 RMJG + 10–15 samples + 2 RMJG + 291 500 + NIST612/NIST614. As there were no matrix-matched primary standards for ilmenite minerals, several known RMs, *i.e.*, zircon 91500, rutile RMJG,[37] and wolframite YGX (Fe-bearing member)[30] and garnet PL-57 (Fe- and Ti-bearing member),[38] were chosen to calibrate the unknowns in experiment 1. In experiments 2 and 3, only zircon 91500 and rutile RMJG were analyzed as primary standards for comparison. Several known ilmenite samples were analyzed to verify the calibration methods.

For the U–Pb dating of garnet, garnet PL-57 was analyzed as the primary standard twice for every 10 or 15 analyses of the tested sample. Mali garnet was used as the secondary standard for monitoring the precision and accuracy of the U–Pb dating results.[26]

The data collected from ICP-MS were processed offline using the ICPMSDataCal software for trace element content and U–Pb age calibration. The detailed calibration equation has been described in previous studies[21,22,31,32] and is also provided as ESI (Table S-1).† Excluding the initial ~2 s, only the first ~25 s of ablation data was used in the calculation to reduce or eliminate down-hole fractionation effects. No additional downhole corrections were employed for Pb/U fractionation. To accurately obtain the U–Pb ages, Ti and Fe elements cannot be analyzed simultaneously with U–Pb isotopes by LA-SF-ICP-MS due to multiple jumps of the magnet for different mass ranges (at least 0.3 s were needed for the jump). Therefore, the semi-quantitative technique of using NIST612 or NIST614 as an external standard was used to obtain U, Th, and Pb contents for ilmenite samples without applying an internal standard. Due to low Pb contents, $^{207}Pb/^{235}U$ and $^{206}Pb/^{238}U$ ratios were used to finish the age calculation. Isoplot 4.15 was used to perform the common Pb correction and calculate lower intercept ages on the Tera-Wasserburg Concordia anchored through age on Concordia (~4950 ± 0.0 Ma) to get a normal initial $^{207}Pb/^{206}Pb$ ratios (~0.84 ± 0.01) according to Stacey and Kramers (1975)[39] or by a well constrained linear array in the Tera–Wasserburg Concordia diagram.[40,41] The final uncertainty of isotopic ratios was calculated as recommended by Horstwood *et al.* (2016).[42]

3. Samples

3.1 Zircon 91500, garnet PL-57, and rutile RMJG

Zircon 91500 contains appropriate U and radiogenic Pb contents of 81 and 14.2 ppm, respectively, with negligible common lead.[43] As the most homogeneous and widely distributed zircon RM in the world, 91500 has a concordant U–Pb age

with a mean $^{206}Pb/^{238}U$ age of 1063.51 ± 0.39 Ma and the isotopic ratios of $^{207}Pb/^{206}Pb = 0.074941 \pm 0.000022$, $^{207}Pb/^{235}U = 1.8525 \pm 0.0012$, and $^{206}Pb/^{238}U = 0.179365 \pm 0.000072$ determined by CA-ID-TIMS and corrected by Horstwood *et al.* (2016).[42]

The PL57 garnet occurs in the calcite ijolite in the Prairie Lake alkaline complex, Canada, and has 6.5–15.0 wt% TiO_2, 17.1–21.3 wt% Fe_2O_3, and 27–76 ppm U; it yielded a concordant ID-TIMS U–Pb age of 1156.2 ± 1.2 Ma.[38]

Rutile RMJG, collected from Palaeoproterozoic pelitic granulites in Hebei Province, China, has low Th, high U, and radiogenic Pb contents of <0.003, ~61, and ~20 ppm, respectively. This rutile yields a weighted mean $^{207}Pb/^{206}Pb$ age of 1751.5 ± 4.3 Ma, $^{206}Pb/^{238}U$ age of 1750.6 ± 8.4 Ma, and $^{207}Pb/^{235}U$ age of 1750.1 ± 4.7 Ma by ID-TIMS and has become a potential reference material.[38]

3.2 Wolframite YGX

Wolframite YGX is from the granite-related Yaogangxian vein-type W deposit in South China. It has been confirmed as a well-characterized RM for wolframite, hübnerite, and scheelite *in situ* U–Pb dating.[30,31] The weighted mean $^{206}Pb/^{238}U$ age of sample YGX by ID-TIMS is 160.9 ± 0.7 Ma.[30]

3.3 Ilmenite samples, HG79 and XL32333

The ilmenite sample, HG79, was from the largest Hongge Fe–Ti–V oxide deposit in the Panzhihua-Xichang district of southwest China. Several world-class magmatic Fe–Ti–V oxide deposits occur here. Titanomagnetite is intergrown with ilmenite to form a massive granular texture in the ores.[44] A ircon $^{206}Pb/^{238}U$ age of 259.3 ± 1.3 Ma had been obtained from the giant Fe–Ti–V ore-bearing Hongge intrusion by ID-TIMS method.[45]

The ilmenite sample, XL32333, was collected from the early Jurassic Fe–Ti oxide-bearing Xialan mafic intrusion in SE China.[13] SHRIMP and Cameca SIMS zircon $^{206}Pb/^{238}U$ age indicate that the Xialan gabbros were emplaced at ~196.0 ± 2.7 Ma.[46–48] Ilmenite is commonly intergrown with magnetite.

3.4 Ilmenite samples, BC28 and BC269

The sample BC28 is a massive magnetite-rich sample from the Magnet Heights location within the Rustenburg Layered Suite in the Bushveld Complex.[17] As a natural Ti-rich magnetite, BC28 has been utilized as a quality control sample for the *in situ* determination of trace elements in magnetite.[49] The sample, BC269, was obtained from a depth of 269.96 m in magnetite diorite from the upper zone of the Bushveld complex.[50] Both BC28 and BC269 were predominately magnetite and contained ilmenite crystals that were hundreds to thousands of microns in size. The Bushveld complex is dated well by zircon and rutile ID-TIMS U–Pb Concordia ages at 2054.4 ± 1.3 and 2055.0 ± 3.9 Ma, respectively.[51] Ilmenite in sample BC28 had U and Pb contents of 48.3 and ~70 ppb, respectively.[17]

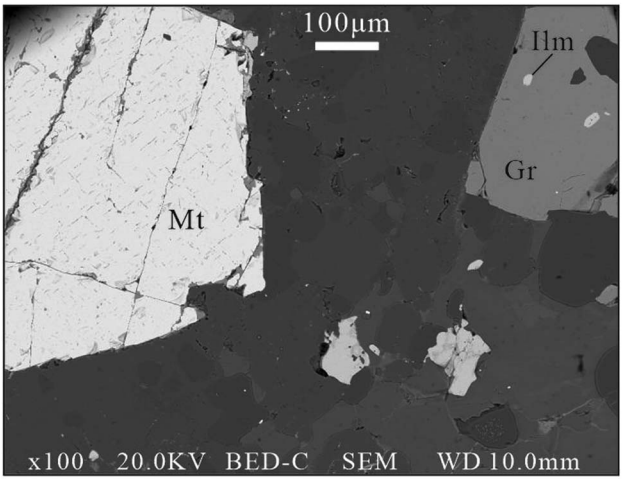

Fig. 1 The intergrowth relationship between magnetite (Mt), ilmenite (Ilm), and garnet (Gr) from the Xikuangshan (XKS) deposit.

3.5 Ilmenite sample, XKS

The ilmenite sample, XKS, was from the Xikuangshan Fe oxide deposit in the northern part of the Kangdian IOCG metallogenic province, China. Metal minerals are dominated by hematite and magnetite with minor ilmenite and chalcopyrite. Disseminated ilmenite grains are intergrown with garnet and magnetite in our samples (Fig. 1). Chalcopyrite samples from the calcite-silication ores, which have a genetic relationship with Fe oxide mineralization, have a Re–Os isotope age of 860.8 ± 22.7 Ma.[52]

4. Results

4.1 U–Pb results in experiment 1

Thirty spots were analyzed for each of the ilmenite samples, HG79, XL32333, and BC269, which contained U concentrations varying from 0.02 to 0.31 ppm (averaging 0.15 ppm), 0.15 to 0.93 ppm (averaging 0.33 ppm), and 0.02 to 0.43 ppm (averaging 0.11 ppm), and total Pb concentrations ranging from 0.01 to 4.03 ppm (averaging 0.16 ppm), 0.02 to 0.05 ppm (averaging 0.03 ppm), and 0.02 to 5.89 ppm (averaging 0.64 ppm) (Table 2), respectively. When using zircon 91500 as a primary standard, ilmenite samples, HG79, XL32333, and BC269, obtained a lower intercept U–Pb age of 262.1 ± 7.7, 199.0 ± 5.3, and 2084 ± 56 Ma in the Tera–Wasserburg Concordia diagram, respectively (Table 2 and Fig. 2). These three samples obtained a lower intercept U–Pb ages of 273.1 ± 7.4, 222.9 ± 6.0, and 2130 ± 58 Ma using garnet PL-57; the ages of 218.2 ± 8.6, 185.7 ± 5.0, and 1848 ± 41 Ma using rutile RMJG; and 297.4 ± 8.5, 254.6 ± 6.8, and 2499 ± 86 Ma using wolframite YGX (Table 2).

4.2 U–Pb results for ilmenite sample, HG79, in experiment 2

More than 30 spots and four-line scanning (with a speed of 1 μm s^{-1}) analyses yielded a lower intercept $^{206}Pb/^{238}U$ age of 260.0 ± 16 Ma (2σ, MSWD = 0.6; Table 3 and Fig. 3a) calibrated by zircon 91500, and 221 ± 13 Ma by RMJG (Table 3) using the spot size of 44 μm, energy density of 4 J cm^{-2}, and repetition rate of 10 Hz.

Table 2 U–Pb results for HG79, XL32333, and BC269 using different primary standards[a]

Ilmenite sample and reference age	U (ppm)	Pb (ppm)	Measured age (Ma) by different primary standard				Age offset (%)
			91500	PL-57	RMJG	YGX	
HG79 (259.3 ± 1.3 Ma)	0.02–0.31 (ave. = 0.15)	0.01–4.03 (0.16)	262.1 ± 7.7	273.1 ± 7.4	218.2 ± 8.6	297.4 ± 8.5	1.1/5.4/16.1/14.9
XL32333 (196.0 ± 2.7 Ma)	0.15–0.93 (0.33)	0.02–0.05 (0.03)	199.0 ± 5.3	222.9 ± 6.0	185.7 ± 5.0	254.6 ± 6.8	1.6/13.9/5.3/30.4
BC269 (2054.4 ± 1.3 Ma)	0.02–0.43 (0.11)	0.02–5.89 (0.64)	2084 ± 56	2130 ± 58	1848 ± 41	2499 ± 86	1.5/3.7/10.2/22.0

[a] Note: (1) HG79 was analyzed as in the ablation setting of 60μm4J6Hz, and the others were analyzed in 60μm4J10Hz; (2) the age offset was calculated using the mathematical equation of $(\mathrm{abs}(A - B))/A \times 100$, where A and B are the ages of the reference and the measured age, respectively; (3) the age offset includes the error which was calculated as recommended by Horstwood *et al.* (2016).[42]

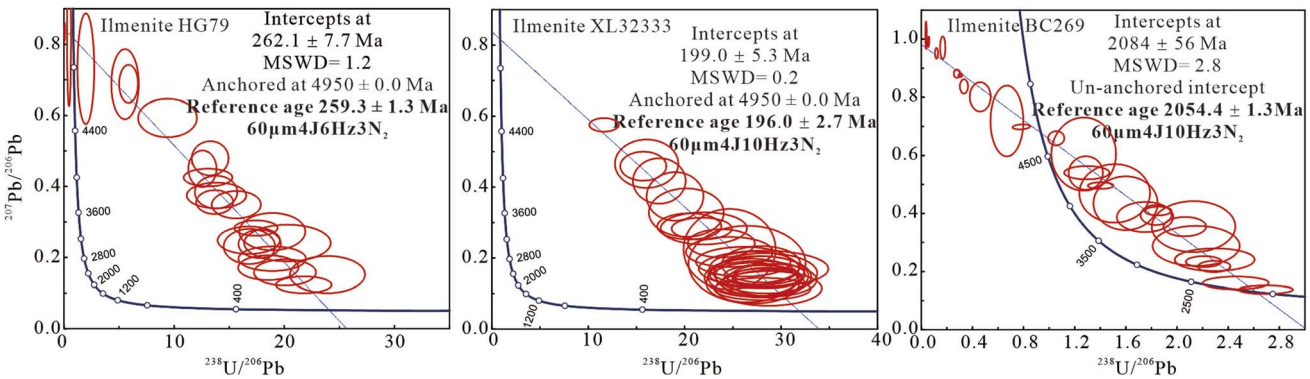

Fig. 2 An accurate lower intercept U–Pb ages was obtained for ilmenite HG79, LX32333, and BC269 using zircon 91500 as a primary standard (data-point error ellipses are 2σ).

Table 3 *In situ* U–Pb ages of ilmenite sample HG79 determined by two primary standards under most possible ablation settings

Ablation settings	Analysis mode	Age (Ma) for HG79		Age offset (%)
		Using 91500	Using RMJG	
Spot: 44μm4J10Hz Line scan: 44 × 1μm10Hz	Spot and line scan	260 ± 16	221 ± 13	0.3/15.0
Spot: 60μm4J6Hz Line scan: 60 × 1μm6Hz	Spot and line scan	256.2 ± 9.2	217.3 ± 8.0	0.0/16.4
Spot: 60μm4J10Hz Line scan: 60 × 1μm10Hz	Spot and line scan	260 ± 12	218.6 ± 9.8	0.3/15.9
Spot: 90μm4J6Hz Line scan: 90 × 1μm6Hz	Spot and line scan	257.3 ± 6.3	209.6 ± 5.1	0.8/19.5
Spot: 120μm3J5Hz Line scan: 120 × 1μm5Hz	Spot and line scan	257.2 ± 8.2	183.4 ± 8.8	0.8/29.7

Thirty spots and six-line scanning (1 μm s^{-1}) analyses yielded a lower intercept $^{206}Pb/^{238}U$ ages of 256.2 ± 9.2 Ma (2σ, MSWD = 0.6; Table 3 and Fig. 3b) upon calibration with zircon 91500, and 217.3 ± 8.0 Ma with RMJG (Table 3) using the spot size of 60 μm, energy density of 4 J cm^{-2}, and repetition rate of 6 Hz.

Twenty-eight spots and four-line scanning (1 μm s^{-1}) analyses yielded a lower intercept $^{206}Pb/^{238}U$ ages of 260.0 ± 12 Ma (2σ, MSWD = 0.7; Table 3 and Fig. 3c) upon calibration with zircon 91500, and 218.6 ± 9.8 Ma with RMJG (Table 3) using the spot size of 60 μm, energy density of 4 J cm^{-2}, and repetition rate of 10 Hz.

More than 23 spots and four-line scanning (1 μm s^{-1}) analyses yielded a lower intercept $^{206}Pb/^{238}U$ ages of 257.3 ± 6.3 Ma (2σ, MSWD = 1.0; Table 3 and Fig. 3d) calibrated by zircon 91500, and 209.6 ± 5.1 Ma by RMJG (Table 3) using the spot size of 90 μm, energy density of 4 J cm^{-2}, and repetition rate of 6 Hz.

Thirty-two spot and five-line scanning (1 μm s^{-1}) analyses yielded a lower intercept $^{206}Pb/^{238}U$ ages of 257.2 ± 8.2 Ma (2σ, MSWD = 1.4; Table 3 and Fig. 3e) calibrated by zircon 91500,

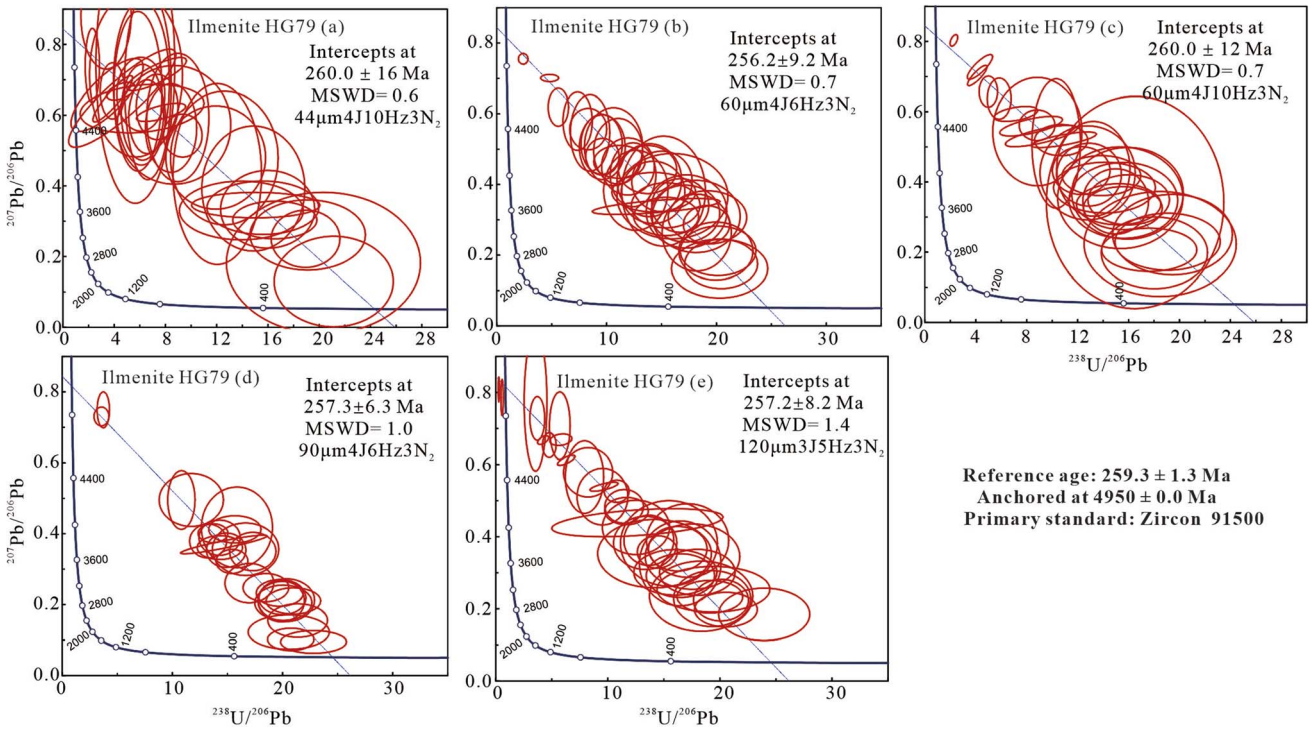

Fig. 3 The lower intercept U–Pb ages was obtained for HG79 using 91500 as the primary standard in most possible ablation settings (data-point error ellipses are 2σ).

Table 4 U–Pb ages for BC28, BC269, LX32333, and XKS samples calibrated by zircon 91500 and rutile RMJG[a]

	Measured ages (Ma) of ilmenite and garnet samples				
	60μm4J6Hz		44μm4J6Hz		32μm4J6Hz
Primary standard	BC28	BC269	LX32333	Ilmenite XKS	Garnet XKS
U (ppm)	0.01–0.66 (0.18)	—	—	0.10–0.57 (0.30)	—
Pb (ppm)	0.09–1.16 (0.39)	—	—	0.04–0.17 (0.07)	—
Using 91500	2052 ± 73	2077 ± 63	198.2 ± 8.8 (1σ)	886 ± 40	—
Using RMJG	1705 ± 52	1697 ± 61	157.7 ± 6.8 (1σ)	681 ± 34	—
Using PL-57	—	—	—	—	881.0 ± 21
Age offset (%)	0.1/17.3	1.1/17.7	1.1/19.8	0.6/23.0	—

[a] Note: the uncertainty of data for LX32333 was 1σ due to low U and Pb contents and used a relatively small spot size; the age offset for ilmenite XKS was calculated against the age of 881.0 ± 21 Ma for garnet XKS.

and 183.4 ± 8.8 Ma by RMJG (Table 3) using a spot size of 120 μm, energy density of 3 J cm^{-2}, and repetition rate of 5 Hz.

4.3 U–Pb results in experiment 3

Using a spot size of 60 μm, energy density of 4 J cm^{-2}, and repetition rate of 6 Hz, 24 spot analyses for BC28 and 25 spot analyses for BC269 yielded a lower intercept $^{206}Pb/^{238}U$ ages of 2052 ± 73 Ma (2σ, MSWD = 0.5; Table 4 and Fig. 4a) and 2077 ± 63 Ma (2σ, MSWD = 1.0; Table 4 and Fig. 4b) calibrated by zircon 91500, and 1705 ± 52 and 1697 ± 61 Ma by RMJG (Table 4), respectively.

Using a small spot size of 44 μm, energy density of 4 J cm^{-2}, and repetition rate of 6 Hz, the ilmenite sample, LX32333 and XKS, yielded a lower intercept $^{206}Pb/^{238}U$ ages of 198.2 ± 8.8 Ma (1σ, MSWD = 0.9; Table 4 and Fig. 4c) and 886.0 ± 40 (2σ, MSWD = 0.9; Table 4 and Fig. 4d) using 91500, and 157.7 ± 6.8, and 681 ± 34 using RMJG (Table 4), respectively. The coexisting garnet obtained a lower intercept $^{206}Pb/^{238}U$ ages of 881.0 ± 21 Ma (2σ, MSWD = 1.5; Table 4 and Fig. 4e).

More than 20 spots were analyzed for the ilmenite samples, BC28 and XKS, which contained U concentrations varying from 0.01 to 0.66 ppm (averaging 0.18 ppm) and 0.10 to 0.57 ppm (averaging 0.30 ppm), and the total Pb concentrations ranging from 0.09 to 1.16 ppm (averaging 0.39 ppm) and 0.04 to 0.17 ppm (averaging 0.07 ppm), respectively.

5. Discussion

5.1 $^{206}Pb/^{238}U$ fractionation for several non-matrix-matched RMs and ilmenite BC269

Suitable matrix-matched standards are preferred to non-matrix-matched standards because they have similar composition and ablation characteristics as the unknowns and can simultaneously correct for mass bias, instrumental drift, and laser-induced elemental fractionation (also known as down-hole fractionation).[35,53] However, such ideal standards have several critical requirements, *e.g.*, abundant reserves for wide distribution, appropriate U and Pb contents to ensure sufficient signals, similar composition and ablation characteristics to match well with the unknown materials, high radiogenic Pb with negligible common Pb to ensure isotopic homogeneity in traditional calibration methods that involve as zircon, or containing variable common Pb, while ensuring age homogeneity as calcite WC-1 and MAD apatite (concordant in the U/Pb systems following common Pb correction).[41,54,55] Thus, such completely homogeneous matrix-matched standards are difficult to find for *in situ* U–Pb dating of new minerals. Meanwhile, matrix effects also exist among matrix-matched minerals (*e.g.*, zircon and apatite) due to minor differences in physical and chemical compositions, *e.g.*, the degree of accumulated radiation damage, trace element composition, and crystallographic orientation, which can lead to different Pb/U fractionation and systematic age bias.[35,36,53,56–58] Moreover, an inhomogeneous matrix-matched standard can also produce an inaccurate age for the unknowns, *e.g.*, with an age offset of ~3% for the apatite sample, calibrated by Otter Lake apatite[53] and ~12% for wolframite samples HG and KA-18, calibrated by concordant wolframite MTM.[59]

Due to the lack of matrix-matched standards, successful LA-ICP-MS U–Pb dating analyses show that homogeneous and widely distributed non-matrix-matched standards were also effective for a growing number of new minerals to yield highly accurate isotopic ratios and ages with some assistant methods or *via* optimizing ablation settings to reduce matrix effects.[17,21,24,25,27,31,32,57] Therefore, non-matrix-matched standards play an important role in U–Pb dating methods, especially when they have U/Pb fractionation similar to that of the unknown materials, and fit all or most of the ablation settings, *e.g.*, wolframite YGX for scheelite,[31] xenotime XN01 for bastnaesite,[32] and zircon 91500 for rutile.[25]

In this analysis, zircon 91500 and three Ti- and Fe-bearing minerals of rutile RMJG, garnet PL-57, and wolframite YGX were selected to match the ilmenite samples. Zircon 91500 has low Ti and Fe contents at ppm level; Rutile contains TiO_2 contents up to 100%, which is much higher than 52.7% in ilmenite; Wolframite YGX contains FeO contents varying from 8.73–9.76 wt%,[60] which is much lower than that in ilmenite. Thus, theoretically, zircon, rutile, and YGX do not match the ilmenite well. In contrast, as a Ti- and Fe-bearing natural mineral, garnet PL-57 has a similar composition (6.5–15.0 wt% TiO_2, 17.1–21.3 wt% Fe_2O_3, and 27–76 ppm U) with ilmenite relative to other RMs.

Rutile TB-1 has been previously utilized to calibrate the Pb/U ratios of four ilmenite minerals to produce accurate U–Pb ages within analytical uncertainties owing to having similar

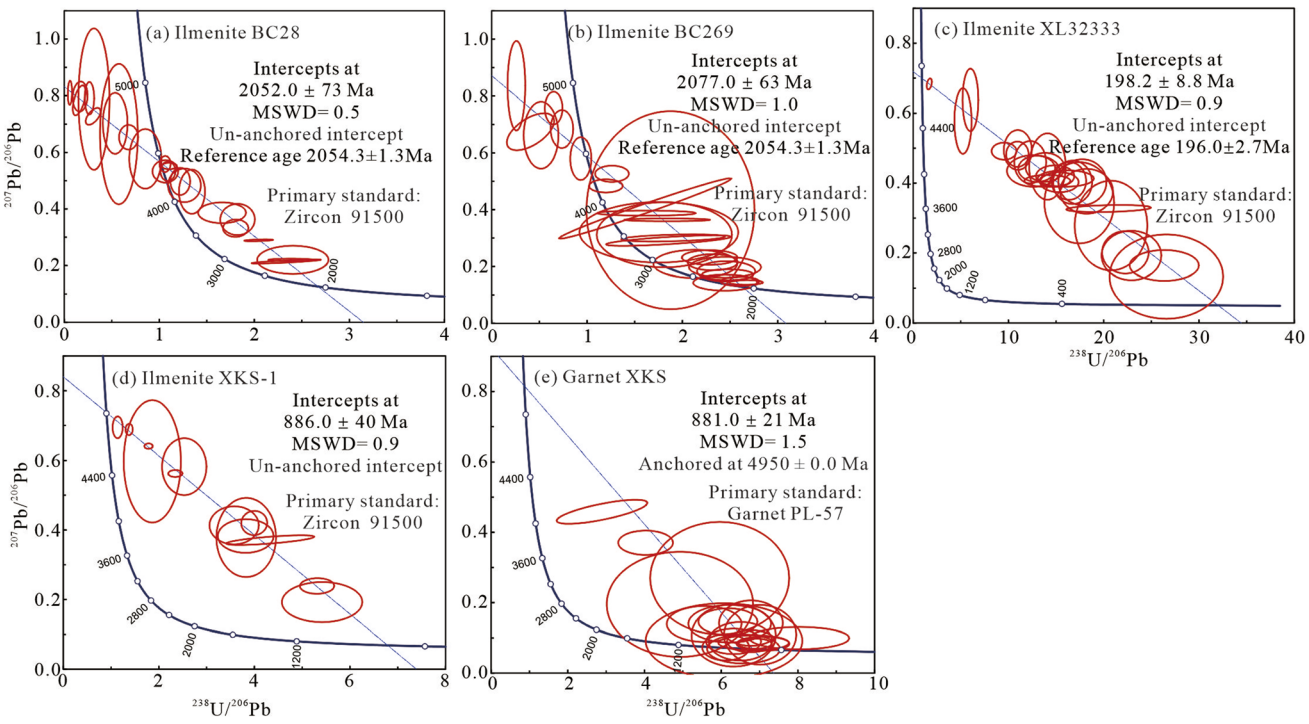

Fig. 4 The lower intercept U–Pb ages were obtained for ilmenite samples and garnet XKS using zircon 91500 and PL-57 as the primary standard, respectively (data-point error ellipses are 2σ).

$^{206}Pb/^{238}U$ isotopic fractionation with ilmenite in an optimized analysis condition of 100μm5J10Hz1.5N_2.[17] Meanwhile, zircon Mud Tank was excluded due to its different U–Pb fractionation under the ablation settings of 100μm2, 3, 5J10Hz1.5N_2.[17] However, zircon 91500 presented similar U–Pb fractionation with rutile in ablation settings of 44, 60, 90μm10J10Hz and without the use of additional nitrogen to increase sensitivity.[25]

In our analysis, there was a slight Pb/U downhole fractionation for each mineral under the two ablation settings of 60μm4J6Hz3N_2 and 60μm4J10Hz3N_2 as shown in Fig. 5, although only ~25 s of the data were used. In contrast, the Pb/U downhole fractionation of rutile, zircon, and ilmenite in the previous study was more serious.[17] BC269 has a similar U–Pb fractionation with 91500 and PL-57, instead of RMJG and YGX. The average normalized Pb/U (Av. Pb/U_N) ratios for each mineral and offsets of four RMs against the corresponding ratios of 0.9683 and 1.7024 for BC269 were calculated. 91500 had an equal value of 0.9596 and 1.6937 with BC269, with an offset of 0.90% and 1.21% (Fig. 5a and b), respectively. The Pb/U fractionation, average Pb/U_N ratio, and offset were consistent with the relationship between their Pb/U downhole fractionation curves, indicating that the matrix effects between BC269 and 91500 were negligible in such analyzed conditions. Moreover, PL-57 had a similar average Pb/U_N ratio of 0.9432 with an offset of 2.59% (Fig. 5a), indicating a potential primary RM. RMJG presented both larger average Pb/U_N ratios of 1.0969 and 2.0656 (Fig. 5a and b), and YGX had a smaller average Pb/U_N ratio of 0.8003, confirming that a matrix effect existed between BC269 and them.

In contrast, zircon, rutile, and ilmenite had an inconsistent U–Pb fractionation in Hou *et al.* (2020),[25] Thompson *et al.* (2021),[17] and our analyses. As mentioned above, the analyzed conditions, including shorter wavelength ablation, spot size, sampling rate and time, energy density, and the addition of assistant materials, such as H_2O, H_2, and N_2, played an important role in changing U/Pb fractionation.[21–23,25,32–34] Both GeoLas and Resolution laser systems in the three analyses were operated at 193 nm wavelength. Thus, the laser system was likely not the principal cause. Other different ablation settings were found, including nitrogen (0.0, 1.5, and 3.0 mL min^{-1}, respectively), spot size-repetition rate-laser fluence (*i.e.*, a fixed ablation setting of 100μm10Hz and 10J10Hz in the two previous studies),[17,25] and effective sampling times (~38, 27.5, and 25 s, respectively). Thus, the variable ablation settings in each study were likely the principal cause for such inconsistent U–Pb fractionation. However, this conclusion needs more experiments for comparison, *i.e.*, using the same RMs and ablation settings in the two laser systems.

In our analysis, two major approaches of optimizing ablation settings and adding N_2 (~3.0 mL min^{-1}) were used to minimize the matrix effects between zircon 91500 and ilmenite. Thus, zircon 91500 could be utilized as a reference material to measure the Pb/U ratio in ilmenite. Summarily, zircon 91500 had similar U–Pb fractionation and average normalized Pb/U ratio as ilmenite BC269, instead of rutile RMJG, probably owing to the different ablation settings used by us compared to the two previous studies.

5.2 A suitable primary standard for *in situ* U–Pb dating of ilmenite samples

Zircon 91500 is the most homogeneous and widely distributed RM and has been approved as a reliable primary standard for *in situ* U–Pb dating of zircon worldwide, as well as for garnet, rutile, vesuvianite, and wolframite.[25–28,61,62] In this analysis, four known ilmenite samples, including BC28, BC269, HG79, and LX32333, were analyzed in spot and line-scan (1 μm s^{-1}) analysis modes under the ablation settings of spot sizes from 44 to 120 μm, energy densities of 3 and 4 J cm^{-2}, and repetition rates from 5 to 10 Hz.

Using zircon 91500 as a primary standard, the ilmenite sample, HG79, was analyzed for condition experiments in six

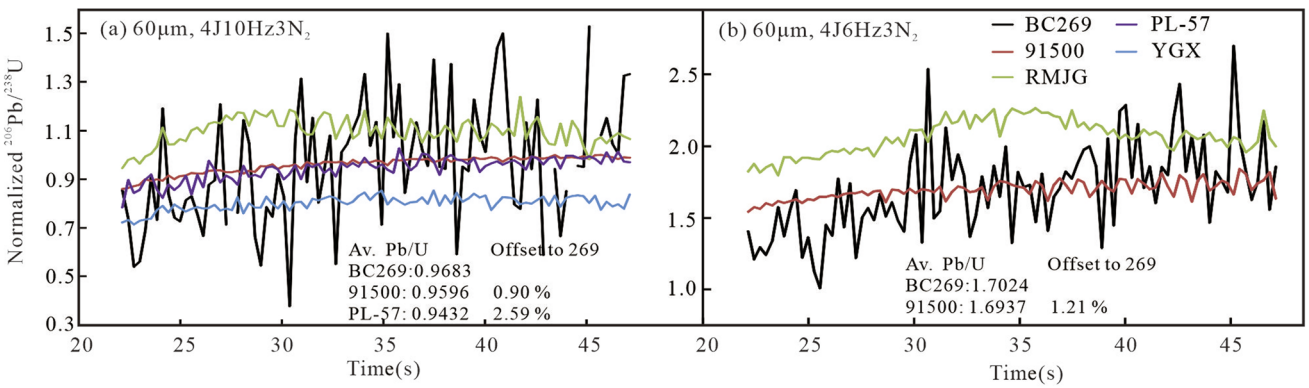

Fig. 5 Normalized $^{206}Pb/^{238}U$ ratio for rutile RMJG, ilmenite BC269, zircon 91500, garnet PL-57, and wolframite YGX. (a) BC269 has a similar U–Pb fractionation with 91500 and PL-57 relative to RMJG and YGX at an ablation setting of 60μm4J10Hz3N_2, and these materials have an average normalized Pb/U ratio of 0.9683, 0.9596, 0.9432, 1.0969, and 0.8003, respectively; (b) BC269 has a similar U–Pb fractionation with 91500 relative to RMJG at an ablation setting of 60μm4J6Hz3N_2, and the three materials has an average normalized Pb/U ratio of 1.7024, 1.6937, and 2.0656, respectively. Note: (1) Pb/U ratio normalized to the published or expected value for each material; (2) excluded first 2.0 seconds, about the next 25 seconds of spot data were used; (3) to exclude the effect from variable common lead, only several BC269 plots with negligible common lead were used.

ablation settings, excluding high energy densities of >5 J cm^{-2} and yielded lower intercept $^{206}Pb/^{238}U$ ages of 262.1 ± 7.7, 260.0 ± 16, 256.2 ± 9.2, 260.0 ± 12, 257.3 ± 6.3, and 257.2 ± 8.2 Ma (Tables 2 and 3). Those ages agree well with the reference age of 259.3 ± 1.3 Ma (ref. 45) within analytical uncertainties and have an age offset of ≤1.1% (Fig. 6a). Other ilmenite samples, XL32333, BC28, and BC269, yielded an accurate lower intercept $^{206}Pb/^{238}U$ ages, which agree well with the published zircon U–Pb age of 196.0 ± 2.7 Ma (ref. 48) and 2054.4 ± 1.3 Ma within errors,[51] respectively, with an age offset of ≤1.6% (Tables 2, 4 and Fig. 6b). These robust ages obtained here confirm that zircon 91500 is a suitable primary standard that fits a wide range of ablation settings for ilmenite minerals.

When using rutile RMJG as the primary standard, the ages mentioned above became significantly younger, with most age offsets of ≥10.2% and only one of ≤5.3% (Tables 2–4). These data on age demonstrate that rutile RMJG is unlikely to be a reliable RM for ilmenite under the current ablation settings. Ilmenite, HG79, XL32333, and BC269, were calibrated by wolframite YGX and yielded much older $^{206}Pb/^{238}U$ ages of 297.4 ± 8.5, 254.6 ± 6.8, and 2499 ± 86 Ma, with age offsets of 14.9%, 30.4%, and 22.0% (Table 2), respectively, indicating that YGX was also not a suitable RM for ilmenite.

Using PL-57 as the primary standard, HG79, XL32333, and BC269 yielded lower intercept $^{206}Pb/^{238}U$ ages of 273.1 ± 7.4, 222.9 ± 6.0, and 2130 ± 58 Ma with the age offset of 5.4%, 13.9%, and 3.7% (Table 2), respectively. If age uncertainty was considered, the obtained ages of HG79 and BC269 are nearly consistent with each reference age. Therefore, garnet PL-57 was shown to be inferior to zircon as a U–Pb RM for ilmenite and an optimized ablation setting should be analyzed further.

Collectively, the results for the four ilmenite minerals calibrated by zircon 91500 are better than those by Ti- and Fe-bearing minerals of rutile RMJG, garnet PL-57, and wolframite YGX. Thus, 91500 is a suitable primary standard for ilmenite minerals during the LA-ICP-MS U–Pb dating process in a wide range of ablation settings.

5.3 The reliability of the calibration method and application

A reliable calibration method commonly relies on high-quality RMs and the sample-standard bracketing approach to correct laser-induced U–Pb downhole fractionation and instrument drift in the U–Pb dating of U-bearing minerals.[41,63,64] This traditional (or direct) method uses homogeneous materials to directly calibrate Pb–Pb and U–Pb isotopes and is widely employed in different kinds of minerals, *e.g.*, zircon, rutile, titanite, monazite, garnet, cassiterite, xenotime, bastnaesite.[37,38,59,63–66] Correspondingly, a mineral that has slightly inhomogeneous U–Pb isotopes will only be proposed as quality control during each analytical session.[30,32]

The two-stage calibration method has also become popular in *in situ* U–Pb dating of U-bearing minerals recently due to the lack of homogeneous standards for some minerals, *e.g.*, apatite, calcite, wolframite, and scheelite.[31,41,55,59] Though containing inhomogeneous U–Pb isotopes and variable common lead, some minerals yielded a uniform and well-constrained lower intercept U–Pb age in the Tera–Wasserburg Concordia diagram and can also be exploited as primary and secondary standard in this calibration method, *e.g.*, WC-1 for calcite and discordant YGX/MTM for wolframite and scheelite.[31,55,59] This method utilizes homogeneous RMs (*e.g.*, NIST glasses) to calibrate Pb/Pb ratios and matrix-matched RMs for U/Pb ratios after correcting for common lead.[31,55,59] A similar calibration process can also be finished by the VizualAge U–Pb data reduction package in Iolite.[41,67] Therefore, the choice between the direct and two-stage calibration method mainly depends on the quality of RMs.

Due to the lack of RMs, several known ilmenite minerals were selected as secondary standards (validation RMs) to establish an accurate *in situ* U–Pb dating method for ilmenite minerals in our and the previous analyses.[17] In this analysis, zircon 91500 was employed as the primary standard to directly calibrate the Pb/Pb and U/Pb ratios for four known ilmenite samples (BC28, BC269, HG79, and LX32333) at a wide range of ablation settings (44 to 120 μm-3, 4 J cm^{-2}-5 to 10 Hz). All of them obtained acceptable low intercept U–Pb ages (Tables 2–4 and Fig. 2–4), verifying that our direct calibration method was reliable.

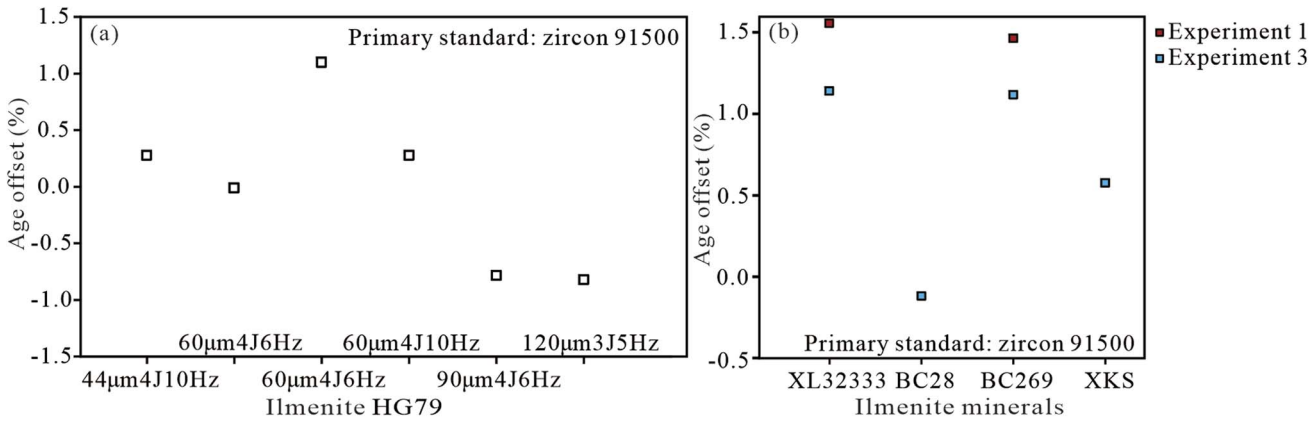

Fig. 6 Age offsets for several ilmenite samples using zircon 91500 as the primary standard. (a) Ilmenite HG79 obtained accurate ages with age offsets of ≤1.1% in five typical ablation settings; (b) four ilmenite samples could obtain accurate ages with age offsets ≤1.6%.

Table 5 U and Pb contents for several ilmenite samples

Ilmenite sample	U (ppm)	Pb (ppm)	Rock or deposit type	References
HG79	0.15	0.16	Fe–Ti–V oxide deposit	This paper
XL32333	0.33	0.03	Xialan mafic intrusion	
BC269	0.11	0.64	Bushveld complex	
BC28	0.18	0.39	Bushveld complex	
XKS	0.30	0.07	Fe oxide deposit	
BC28	0.05	~0.02	Bushveld complex	Thompson *et al.*, 2021 (ref. 17)
Frank smith	0.05	<0.01	Kimberlite	
Monastery	0.07	<0.01	Kimberlite	
Premier	0.01	<0.01	Kimberlite	
Skerring	0.03	~0.03	Kimberlite	

An unknown ilmenite sample was chosen from the Xikuangshan Fe oxide deposit in the northern part of the Kangdian IOCG metallogenic province, China. The edge of well-zoned ilmenite XKS was analyzed in a smaller spot size of 44 μm, which obtained an accurate age of 886 ± 40 Ma (Fig. 4d). This U–Pb age is consistent with the coexisted garnet U–Pb age of 881.0 ± 21 Ma within error (Fig. 1 and 4e), and also agrees well with the younger Re–Os isotope age of 860.8 ± 22.7 Ma for chalcopyrite samples from the copper ore bodies in the Xikuangshan deposit,[52] as well as the U–Pb age of 880–850 Ma for secondary allanite in the Lala Fe–Cu deposit in the same mineralization belt,[68] indicating that the late important Fe mineralization event in the Kangdian region occurred at ~880 Ma.

Summarily, the accurate ages obtained here for five ilmenite samples in the three experiments demonstrate that our established calibration method using 91500 as the external standard is effective for *in situ* U–Pb dating of the ilmenite samples.

5.4 Potential reference materials for *in situ* ilmenite U–Pb dating

Among the nine known ilmenite minerals given in Table 5, all the ilmenite samples from the kimberlite intrusions contain low U and Pb contents varying from 0.01 to 0.07 and <0.01 to 0.03 ppm, respectively, which are nearly at the detection limits of LA-ICP-MS and are difficult to accurately measure unless some special conditions of analysis are applied, *e.g.*, large spot size (compared to a normal spot size of 32 μm), high ablation rate, and adding N_2. In addition, those samples produce spread plots in the Tera–Wasserburg Concordia diagram with most MSWD values of ≥1.6, when calculating the lower intercept U–Pb ages.[17] Thus, they are not suitable as RMs for *in situ* U–Pb dating. In contrast, our selected samples in this analysis had U contents varying from 0.11 to 0.33 ppm, which were about an order of magnitude higher than those in kimberlitic ilmenite samples. Especially, the ilmenite samples, HG79, XL32333, and BC269, were chosen from Fe–Ti oxide deposits or Fe–Ti oxide-bearing mafic intrusions and had relatively abundant reserves. More than 20 spot analyses for each of them produced a robust low intercept U–Pb age in the Tera–Wasserburg Concordia diagram with most MSWD values of ~1.0. Thus, they can be proposed as potential RMs at the moment.

Meanwhile, we note that XL32333 has the lowest lead content relative to the other four samples in our analysis. Thus, it needs a high ratio of the signal relative to background intensity for accurate measurement of ^{206}Pb, and especially, ^{207}Pb. The related approaches include maintaining a relatively low background, enhancing sensitivity by adding a small amount of N_2 (or water vapor, and H_2),[17,20,21,32] and improving Pb signal intensities by using a large spot size.[17,55] BC269 has the highest radiogenic lead due to its oldest formation age of 2054.4 Ma and also needs appropriate ablation settings to fit its moderate to low U contents (0.11 ppm). HG79 has moderate U and Pb contents of ~0.15 ppm and is easy to measure relative to other samples. In addition, BC28 has higher U and Pb contents than those in previous studies and obtained a well-constrained U–Pb age in the Tera–Wasserburg Concordia diagram with a smaller MSWD value of 0.5, indicating inhomogeneous isotopes in diverse grains and unsuitability to be an RM. Therefore, HG79, XL32333, and BC269 have their own advantage in high U and Pb contents, relative to other known ilmenite samples, and they can be utilized as potential RMs for *in situ* U–Pb dating of ilmenite minerals.

6. Conclusions

(1) 91500 and PL-57 have similar U–Pb fractionation and average normalized Pb/U ratio with ilmenite BC269, instead of RMJG and YGX in our analyzed conditions.

(2) Zircon 91500 is a reliable RM for *in situ* U–Pb dating of ilmenite under a wide range of ablation settings.

(3) A reliable direct calibration method was established for *in situ* U–Pb dating of ilmenite minerals.

(4) Ilmenite samples HG79, LX32333, and BC269 contain appropriate U and Pb contents and can be utilized as potential RMs for *in situ* U–Pb dating of ilmenite.

Conflicts of interest

There are no conflicts of interest to declare.

Acknowledgements

This study was financially supported by the National Key Research and Development Program of China (Grant No. 2018YFA0702602), the National Natural Science Foundation of China (Grant No. 42072103, 42122024, 42025301), the 2022

Technical Support Talent Project of the Chinese Academy of Sciences, CAS Hundred Talents Program to XWH, and Guizhou Provincial 2020 Science and Technology Subsidies (No. GZ2020SIG). The authors are thankful to Dr Lei Liu and Prof. Wei Terry Chen for providing the ilmenite sample, XKS. The authors are also thankful to Dr Dany Savard from LabMaTer in the UQAC for providing the ilmenite samples, BC28 and BC269, and Dr Shaohua Dong for helping record the SEM images.

References

1 C. Perks and G. Mudd, *Miner. Econ.*, 2021, **34**, 345–370.
2 U. S. Geological Survey, *Mineral Commodity Summaries*, 2022, pp. 176–179.
3 M. Altunbey and A. Sagiroglu, *J. Asian Earth Sci.*, 2003, **21**, 481–488.
4 T. E. Nowicki, R. O. Moore, J. J. Gurney and M. C. Baumgartner, *Dev. Sedimentol.*, 2007, **58**, 1235–1267.
5 A. S. M. M. Hasan, I. Hossain, M. A. Rahman, M. N. Zaman, P. K. Biswas and M. S. Alam, *Ore Geol. Rev.*, 2022, **141**, 104687.
6 P. A. Schroeder, J. J. Le Golvan and M. F. Roden, *Am. Mineral.*, 2002, **87**, 1616–1625.
7 A. S. M. M. Hasan, I. Hossain, M. A. Rahman, M. S. Rahman, M. N. Zaman and P. K. Biswas, *Arabian J. Geosci.*, 2018, **11**, 1–14.
8 K. B. Prissel, M. J. Krawczynski and J. A. V. Orman, *Contrib. Mineral. Petrol.*, 2020, **175**, 1–17.
9 D. A. B. Unganai, A. Imai, R. Takahashi, D. L. Jamal, A. Agangi, T. Hoshide and H. Sato, *Ore Geol. Rev.*, 2022, **143**, 104760.
10 D. H. A. Cavalcante, L. dos Santos, I. D. Guimaraes, L. D. Batista, B. S. Araujo, J. V. A. de Amorim and G. N. Queiroga, *J. South Am. Earth Sci.*, 2023, **122**, 104159.
11 P. D'Arco and R. C. Maury, *Can. Mineral.*, 1981, **19**, 461–467.
12 N. J. G. Pearce, *Mineral. Mag.*, 1990, **54**, 585–588.
13 Z. J. Bai, W. G. Zhu, H. Zhong, C. Li, J. Q. Liao and H. S. Sun, *Lithos*, 2015, **212**, 59–73.
14 K. W. Burton and R. K. O'Nions, *Geochim. Cosmochim. Acta*, 1990, **54**, 2593–2602.
15 A. K. Noyes, L. M. Heaman and R. A. Creaser, *Dyke Swarms: Keys for Geodynamic Interpretation*, 2011, pp. 457–492.
16 A. N. Halliday, M. Ohr, K. Mezger, J. T. Chesley, S. Nakai and C. P. Dewolf, *Rev. Geophys.*, 1991, **29**, 577–584.
17 J. M. Thompson, K. Goemann, I. Belousov, K. Jenkins, A. Kobussen, W. Powell and L. Danyushevsky, *J. Anal. At. Spectrom.*, 2021, **36**, 1244–1260.
18 B. J. Fryer, S. E. Jackson and H. P. Longerich, *Chem. Geol.*, 1993, **109**, 1–8.
19 M. Guillong and C. A. Heinrich, *J. Anal. At. Spectrom.*, 2007, **22**, 1488–1494.
20 Z. C. Hu, S. Gao, Y. S. Liu, S. H. Hu, H. H. Chen and H. L. Yuan, *J. Anal. At. Spectrom.*, 2008, **23**, 1093–1101.
21 T. Luo, Z. C. Hu, W. Zhang, Y. S. Liu, K. Q. Zong, L. Zhou, J. Zhang and S. Hu, *Anal. Chem.*, 2018, **90**, 9016–9024.
22 T. Luo, H. Zhao, Q. L. Li, Y. Li, W. Zhang, J. L. Guo, Y. S. Liu, J. F. Zhang and Z. C. Hu, *Geostand. Geoanal. Res.*, 2020, **44**, 653–668.
23 C. R. McFarlane, *Chem. Geol.*, 2016, **438**, 91–102.
24 M. Burn, P. Lanari, T. Pettke and M. Engi, *J. Anal. At. Spectrom.*, 2017, **32**, 1359–1377.
25 Z. H. Hou, Y. L. Xiao, J. Shen and C. L. Yu, *J. Asian Earth Sci.*, 2020, **192**, 104261.
26 Y. W. Tang, J. F. Gao, T. G. Lan, K. Cui, J. J. Han, X. Zhang, Y. W. Chen and Y. H. Chen, *Ore Geol. Rev.*, 2021, **130**, 103970.
27 Y. H. Chen, R. Z. Hu, T. G. Lan, H. Wang, Y. W. Tang, Y. H. Yang, Z. D. Tian and T. Ulrich, *Chem. Geol.*, 2021, **572**, 120198.
28 L. Z. Xing, J. T. Peng, Y. J. Lv, Y. W. Tang and J. F. Gao, *Chem. Geol.*, 2022, **607**, 121017.
29 Q. D. Wei, M. Yang, R. L. Romer, H. Wang, Y. H. Yang, Z. F. Zhao, S. T. Wu, L. W. Xie, C. Huang, L. Xu, J. H. Yang and F. Y. Wu, *J. Anal. At. Spectrom.*, 2022, **37**, 69–81.
30 M. Yang, Y. H. Yang, S. T. Wu, R. L. Romer, X. D. Che, Z. F. Zhao, W. S. Li, J. H. Yang, F. Y. Wu, L. W. Xie, C. Huang, D. Zhang and Y. Zhang, *J. Anal. At. Spectrom.*, 2020, **35**, 2191–2203.
31 Y. W. Tang, J. J. Han, T. G. Lan, J. F. Gao, L. Liu, C. H. Xiao and J. H. Yang, *J. Anal. At. Spectrom.*, 2022, **37**, 358–368.
32 Y. W. Tang, N. Liu, J. H. Yang, G. O. Gonçalves, L. Liu, T. G. Lan, J. F. Gao and J. J. Han, *J. Anal. At. Spectrom.*, 2022, **37**, 2599.
33 A. El Korh, *Chem. Geol.*, 2014, **371**, 46–59.
34 S. E. Jackson, N. J. Pearson, W. L. Griffin and E. A. Belousova, *Chem. Geol.*, 2004, **211**, 47–69.
35 E. Marillo-Sialer, J. Woodhead, J. Hergt, A. Greig, M. Guillong, A. Gleadow, N. Evans and C. Paton, *J. Anal. At. Spectrom.*, 2014, **29**, 981–989.
36 J. Thompson, S. Meffre and L. Danyushevsky, *J. Anal. At. Spectrom.*, 2018, **33**, 221–230.
37 L. Zhang, J. L. Wu, J. R. Tu, D. Wu, N. Li, X. P. Xia and Z. Y. Ren, *Geostand. Geoanal. Res.*, 2020, **44**, 133–145.
38 D. F. Li, Y. Fu, P. Hollings, R. Mitchell, S. Zurevinski, S. Kamo, R. Q. Zhang, Y. Zhang, Q. F. Liu, J. L. Liao and Y. J. Liang, *Contrib. Mineral. Petrol.*, 2022, **177**, 19.
39 J. S. Stacey and J. D. Kramers, *Earth Planet. Sci. Lett.*, 1975, **26**, 207–221.
40 D. M. Chew, P. J. Sylvester and M. N. Tubrett, *Chem. Geol.*, 2011, **280**, 200–216.
41 D. M. Chew, J. A. Petrus and B. S. Kamber, *Chem. Geol.*, 2014, **363**, 185–199.
42 M. S. A. Horstwood, J. Kosler, G. Gehrels, S. E. Jackson, N. M. McLean, C. Paton, N. J. Pearson, K. Sircombe, P. Sylvester, P. Vermeesch, J. F. Bowring, D. J. Condon and B. Schoene, *Geostand. Geoanal. Res.*, 2016, **40**, 311–332.
43 M. Wiedenbeck, P. AllÉ, F. Corfu, W. L. Griffin, M. Meier, F. Oberli, A. V. Quadt, J. C. Roddick and W. Spiegel, *Geostand. Newsl.*, 1995, **19**, 1–23.
44 Z. J. Bai, H. Zhong, R. Z. Hu and W. G. Zhu, *Econ. Geol.*, 2021, **116**(3), 681–691.
45 H. Zhong and W. G. Zhu, *Miner. Deposita*, 2006, **41**, 599–606.

46 X. Q. Yu, Y. J. Di, G. G. Wu, D. Zhang, Y. Zheng and Y. P. Dai, *Sci. China, Ser. D: Earth Sci.*, 2009, **52**(4), 471–483.
47 W. G. Zhu, H. Zhong, X. H. Li, D. F. He, X. Y. Song, T. Ren, Z. Q. Chen, H. S. Sun and J. Q. Liao, *Lithos*, 2010, **119**, 313–329.
48 C. S. Gan, Y. J. Wang, X. Qian, M. W. Bi and H. Y. He, *J. Asian Earth Sci.*, 2017, **145**, 576–590.
49 S. A. S. Dare, S. J. Barnes, G. Beaudoin, J. Méric, E. Boutroy and C. Potvin-Doucet, *Miner. Deposita*, 2014, **49**, 785–796.
50 S. J. Barnes, W. D. Maier and L. D. Ashwal, *Chem. Geol.*, 2004, **208**, 293–317.
51 J. S. Scoates and R. M. Friedman, *Econ. Geol.*, 2008, **103**, 465–471.
52 Y. L. Li, *A Dissertation Submitted for the Degree of Master of Science*, Kunming University of Science and Technology, 2013, pp. 54–55.
53 J. Thompson, S. Meffre, R. Maas, V. Kamenetsky, M. Kamenetsky, K. Goemann, K. Ehrig and L. Danyushevsky, *J. Anal. At. Spectrom.*, 2016, **31**, 1206–1215.
54 X. H. Li, G. Q. Tang, B. Gong, Y. H. Yang, K. J. Hou, Z. H. Hu, Q. L. Li, Y. Liu and W. X. Li, *Chin. Sci. Bull.*, 2013, **58**, 4647–4654.
55 N. M. W. Roberts, E. T. Rasbury, R. R. Parrish, C. J. Smith, M. S. A. Horstwood and D. J. Condon, *Geochem., Geophys., Geosyst.*, 2017, **18**, 2807–2814.
56 S. M. Eggins, L. P. J. Kinsley and J. M. G. Shelley, *Appl. Surf. Sci.*, 1998, **127–129**, 278–286.
57 L. P. Black, S. L. Kamo, C. M. Allen, D. W. Davis, J. N. Aleinikoff, J. W. Valley, R. Mundil, I. H. Campbell, R. J. Korsch, I. S. Williams and C. Foudoulis, *Chem. Geol.*, 2004, **205**, 115–140.
58 E. Marillo-Sialer, J. Woodhead, J. M. Hanchar, S. M. Reddy, A. Greig, J. Hergt and B. Kohn, *Chem. Geol.*, 2016, **438**, 11–24.
59 Y. W. Tang, K. Cui, Z. Zheng, J. F. Gao, J. J. Han, J. H. Yang and L. Liu, *Gondwana Res.*, 2020, **83**, 217–231.
60 X. D. Deng, T. Luo, J. W. Li and Z. C. Hu, *Chem. Geol.*, 2019, **515**, 94–104.
61 X. D. Deng, J. W. Li, T. Luo and H. Q. Wang, *Contrib. Mineral. Petrol.*, 2017, **172**, 71.
62 T. Luo, X. D. Deng, J. W. Li, Z. C. Hu, W. Zhang, Y. S. Liu and J. F. Zhang, *J. Anal. At. Spectrom.*, 2019, **34**, 1439–1446.
63 Y. S. Liu, Z. C. Hu, K. Q. Zong, C. G. Gao, S. Gao, J. Xu and H. H. Chen, *Chin. Sci. Bull.*, 2010, **55**, 1535–1546.
64 Y. H. Yang, F. Y. Wu, Y. Li, J. H. Yang, L. W. Xie, Y. Liu, Y. B. Zhang and C. Huang, *J. Anal. At. Spectrom.*, 2014, **29**, 1017–1023.
65 A. D. Vasconcelos, G. O. Gonçalves, C. Lana, I. S. Buick, S. L. Kamo, F. Corfu, R. Scholz 1, A. Alkmim, G. Queiroga and H. A. Nalini Jr, *Geostand. Geoanal. Res.*, 2018, **19**, 2262–2282.
66 A. K. Kenedy, S. L. Kamo, L. Nasdala and N. E. Timms, *Can. Mineral.*, 2010, **48**, 1423–1443.
67 J. A. Petrus and B. S. Kamber, *Geostand. Geoanal. Res.*, 2012, **36**, 247–270.
68 W. T. Chen and M. F. Zhou, *Contrib. Mineral. Petrol.*, 2014, **168**, 1043.